The copper(II) and zinc(II) coordination mode of HExxH and HxxEH motif in small peptides: The role of carboxylate location and hydrogen bonding network

Giuseppe Grasso [a], Antonio Magrì [b], Francesco Bellia [b], Adriana Pietropaolo [c,*],
Diego La Mendola [d,**], Enrico Rizzarelli [a]

[a] *Dipartimento di Scienze Chimiche, Università degli Studi di Catania, Viale A. Doria 6, 95125 Catania, Italy*
[b] *Istituto di Biostrutture e Bioimmagini, Consiglio Nazionale delle Ricerche (CNR) Catania, Viale A. Doria 6, 95125 Catania, Italy*
[c] *Dipartimento di Scienze della Salute, Università di Catanzaro, Viale Europa, 88100 Catanzaro, Italy*
[d] *Dipartimento di Farmacia, Università di Pisa, Via Bonanno Pisano 6, 56126 Pisa Italy*

ABSTRACT

Copper(II) and zinc(II) complexes with two hexapeptides encompassing HExxH and HxxEH motif were characterized by means of a combined experimental and theoretical approach. Parallel tempering and density functional theory (DFT) investigations show the presence of different hydrogen bonding networks between the copper(II) and zinc(II) complexes with the two peptides, suggesting a significant contribution of these non-covalent interactions to the stability constant values. The glutamate carboxylate group has a direct role in metal ion binding. The location of this amino acid along the sequence of the investigated peptides is critical to determine thermodynamic and spectroscopic features of the copper(II) complex species, whereas is less relevant in the zinc(II) complexes formation. Electrospray ionization mass spectrometry (ESI-MS) characterization of the zinc(II) complex species show that in the $[ZnH_{-2}L]$ two deprotonated amide nitrogen atoms are involved in the metal coordination environment, an uncommon behavior in zinc(II) complexes for multi-histidine ligands.

© 2013 Elsevier Inc. All rights reserved.

1. Introduction

The high frequency of occurrence of a single amino acid in proteins characterizes the so-called "Xaa-rich" proteins (Xaa here refers to any type of amino acids). The physiological and pathological roles of cysteine- [1,2], glutamine- [3,4], glycine- [5,6], leucine- [7,8] and proline-rich [9–11] proteins with their sequence repeats have been reported. Although the average frequency of occurrence of histidine in all proteins is relatively low [12], the histidine-rich proteins are probably the most noticeable ones among the "Xaa-rich" proteins [13–19]. The versatility of histidine coordination favors transition metal bindings and many studies have been focused on characterizing the metal interactions with sequentially histidine-rich motifs/proteins. However, proteins with inconsecutive histidines in primary sequences are also able to form local histidine-rich environments as consequence of the folding process, so that the metal ions can be coordinated [20–24]. Among the large quantity of metalloproteins which employ histidine residues for metal coordination, almost all copper-binding histidine rich proteins comprise only histidines as partners in metal interactions [12].

Copper complexes of linear and cyclic multi-histidine peptides have been the focus of numerous studies with the aims to understand the stabilizing role of histidyl residues in the active center of copper proteins [25–36]. The general features of the complex formation reactions and the coordination mode of this metal ion with His-containing peptides have been reviewed by several authors [37–39]. For multi-histidine peptides with protecting groups at the N- and C-termini, there is general agreement that: i) the metal ion speciation and the coordination modes are driven by the number and the position of the His residues in the peptide sequences; ii) the coordination modes of the major species are generally described by the formation of 5-, 6- or 7-membered chelates including the imidazole and deprotonated amide nitrogens; iii) the metal binding of deprotonated amide nitrogens starts from the internal histidine anchoring residue and is followed by the subsequent amino acids towards the N-terminus favoring the (6,5,6)-membered chelate formation; iv) the increase in the number of histidine residues favors the formation of macrochelates in slightly acidic and/or neutral solution as found in large peptide fragments of natural proteins including prions, histones and amyloid peptides [40–44]; v) both thermodynamic and spectroscopic data indicate the existence of coordination isomers in solution.

The formation of macrochelates has also been reported for zinc(II) complexes with multihistidine peptides [35,36,45–49], while the ability of zinc(II) to promote amide nitrogen deprotonation has only been observed in few cases and above pH 7 [35,45,46].

On the other hand, the results of a recent bioinformatics approach exploring histidine-rich clusters in proteins [12] indicate that Zn^{2+} and Fe^{2+} show slightly preference towards histidine with acidic aspartic acid or glutamic acid residue as ligand group. For enzyme relying on mononuclear metal cofactors, the so-called Facial Triad Motif, combining two histidines and one carboxylate (either aspartate or glutamate) has emerged as a recurring and versatile motif [50]. Many three-dimensional structures of metallopeptidases have been resolved and the larger superfamily of zinc(II) metalloproteases is featured by the HExxH motif that is present in many zinc peptidases (zincins) [51]. Similar to other M16 family proteases, insulin degrading enzyme (IDE) shows the zinc binding motif of inverzincins HxxEH, that is inverted to the canonical metallo-proteases motif. In recent years, we have demonstrated that diverse biomolecules as well as metal ions are able to modulate IDE activity [52–56]. Particularly, it has been demonstrated that copper(I) as well as copper(II) have a strong inhibitory role towards the degradation of insulin [57] and Aβ [58] peptides by IDE. However, while the inhibition by copper(I) has been shown to be irreversible, copper(II) inhibition could be reversed by the addition of a zinc(II) excess. Unbiased molecular dynamic simulations predicted that, in the case of copper(I), the metal ion binding to the two cysteines Cys812 and Cys819 of IDE restricts the access of the substrate to the catalytic cavity [59]. On the other hand, it has been speculated that copper(II) could substitute the zinc ion inside the catalytic chamber, somehow hindering the proteolytic function of the enzyme. Indeed, as the coordination modes of copper(II) and zinc(II) in peptides are generally different, a distortion of the catalytic site is very much expected upon substitution of the coordinated metal ion. Copper(II) shows a higher affinity than zinc(II) for the imidazole nitrogen atoms of peptide ligands that form macrochelate rings, so it is plausible to conclude that the added Cu^{2+} substitutes Zn^{2+} in the catalytic site, bringing about the inhibition of enzyme activity due to the different coordination requirements of the two metal ions. Such hypothesis is supported by the observation that the substitution of the zinc ions of the catalytic sites in zinc metalloproteases by other divalent cations usually produces large effect on their structure and catalytic activity [59]. This is the case of metalloproteases such as thermolysin [60], carboxypeptidase A [61], endopeptidase from *Lactococcus lactis* [62] or aminopeptidase B [63] which lose their activity upon zinc(II) substitution with copper(II). However, other zinc proteases such as dipeptidyl peptidase and astacin show high metal substitution tolerance [64]. In this scenario, the amount of literature data on zinc complexes with peptides containing histidine and aspartic acid or glutamic acid residues is not enough to understand all aspects of these interactions [45].

Here we report the results on the zinc(II) and copper(II) complexes with two model peptides, containing the zinc binding motif of the two families of metallopeptidases, Ac-GHEITHG-NH2 (zincin-motif) and Ac-GHTIEHG-NH2 (inverzincin-motif) (Chart 1). The selection of these ligands made possible to study the effect of the carboxylate residue in different locations in respect to the two histidine residues, by means of a combined potentiometric, spectroscopic and computational approaches.

2. Experimental

2.1. Materials

All N-fluorenylmethoxycarbonyl (Fmoc)-protected amino-acids and 2-(1-H-benzotriazole-1-yl)-1,1,3,3-tetramethyluronium tetrafluoroborate (TBTU) were obtained from Novabiochem (Switzerland); Fmoc-PAL-PEG resin, N,N-diisopropyl-ethylamine (DIEA), N,N-dimethylformamide (DMF, peptide synthesis grade) and 20% piperidine-DMF solution were from Applied Biosystems;
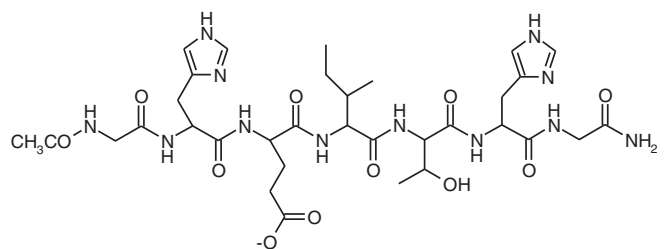
Ac-GHEITHG-NH2 (zincin-motif)
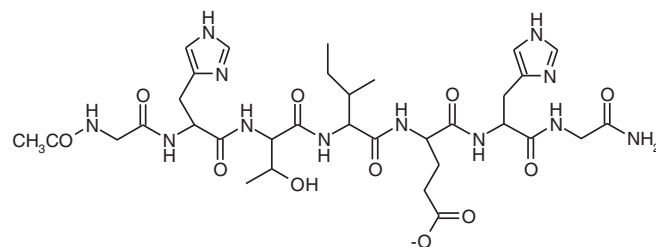
Ac-GHTIEHG-NH2 (inverzincin-motif)

Chart 1. Schematic view of primary sequences of peptides investigated.

N-hydroxybenzotriazole (HOBT), triisopropylsilane (TIS), and trifluoroacetic acid (TFA) were purchased from Sigma/Aldrich. All the other chemicals were of the highest available grade and were used without further purification.

2.2. Peptide synthesis and purification

The peptides Ac-GHEITHG-NH2 and Ac-GHTIEH-NH2 were assembled using the solid phase peptide synthesis strategy on a Pioneer™ Peptide Synthesiser. All amino acid residues were added according to the TBTU/HOBT/DIEA activation method for Fmoc chemistry on Fmoc-PAL-PEG resin (loading 0.22 mmol/g, 0.33 mmol scale synthesis, 1.5 g of resin). Other experimental details have already been reported [65].

The peptides were purified by means of a preparative reversed-phase (rp)-HPLC. Purification was performed on a Varian PrepStar 200 model SD-1 chromatography system equipped with a Prostar photodiode array detector with detection at 222 nm. They were eluted with solvent A (0.1% TFA in water) and B (0.1% TFA in acetonitrile) on a Vydac C18 250 × 22 mm (300 Å pore size, 10–15 μm particle size) column, at a flow rate of 0.2 mL/min. Analytical rp-HPLC analyses were performed using a Agilent 1200 series instrument, equipped with a DAD detector. Samples were analyzed using gradient elution with solvent A and B on a Vydac C18 250 × 4.6 mm (300 Å pore size, 5 μm particle size) column, at a flow rate of 1 mL/min. The peptides were eluted according to the following protocol: from 0 to 5 minutes isocratic gradient in 0% B, then linear gradient from 0 to 10% B over 15 min, finally isocratic gradient in 10% B from 15 to 30 min. Peptides were characterized by means of electrospray ionization mass spectrometry (ESI-MS).

Ac-GHEITHG-NH2: [R_t = 21.4 min]. Calculated mass for $C_{33}H_{50}N_{12}O_{11}$ M = 790.37, ESI-MS [Obsd m/z: $(M + H)^+$ 791.4].
Ac-GHTIEHG-NH2: [R_t = 22.0 min]. Calculated mass for $C_{33}H_{50}N_{12}O_{11}$ M = 790.37, ESI-MS [Obsd m/z: $(M + H)^+$ 791.4].

2.3. Potentiometric titrations

Potentiometric titrations were performed with two home-assembled fully automated apparatus sets (Metrohm E654 pH-meter, combined micro pH glass electrode, Orion 9103SC, Hamilton digital dispenser,

Model 665) controlled by the appropriate software set up in our laboratory [66]. The titration cell (2.5 ml) was thermostated at 298.0 ± 0.2 K, and all solutions were kept under an atmosphere of argon, which was bubbled through a solution having the same ionic strength and temperature as the measuring cell. KOH solutions (0.1 M) were added through a Hamilton buret equipped with 1 cm^3 syringes. The ionic strength of all solutions was adjusted to 0.10 M (KNO_3). To determine the stability constants, solutions of the ligands (protonation constants) or the ligands with Cu^{2+} (copper(II) complex constants) and with Zn^{2+} (zinc(II) complex constants) were titrated by using 0.1 M potassium hydroxide. The peptide concentration ranged from 1.0 to 3.0×10^{-3} and from 1.0 to 4.0×10^{-3} M for the protonation and complexation experiments, respectively. The initial pH was always adjusted to 2.4. Stability constants for proton complexes were calculated from three peptide titrations carried out over the pH range 2.3–9.0. Triplicate titrations were performed to determine the Cu^{2+} complex stability constants in the pH range 2.5–8.0 while the zinc(II) complex formation was investigated in the pH range 2.5–7.2. To avoid systematic errors and verify reproducibility, the electromotive force (EMF) values of each experiment were taken at different time intervals. To obtain protonation and complexation constants, the potentiometric data were refined using the HYPERQUAD program [67], which minimizes the error square sum of the measured electrode potentials through a nonlinear iterative refinement of the sum of the squared residuals, U, and also allows for the simultaneous refinement of data from different titrations:

$$U = \Sigma \left(E_{exp} - E_{calc} \right)^2.$$

E_{exp} and E_{calc} are the experimental and calculated electrode potentials, respectively. Errors in stability constant values are reported as three times the standard deviations.

The formation reaction equilibria of ligands with protons and metal ions are given in Eq. (1):

$$pM + qH + rL = M_p H_q L_r \tag{1}$$

in which L is the peptide under study. The stability constant β_{pqr} is defined in Eq. (2):

$$\beta_{pqr} = \left[M_p H_q L_r \right] / [M]^p \cdot [H]^q \cdot [L]^r. \tag{2}$$

The species distribution as a function of the pH was obtained by using the computer program Hyss [68].

2.4. Spectroscopic studies

2.4.1. UV–visible (UV–vis) measurements

UV–visible (UV–vis) spectra were recorded at 25 °C, by using an Agilent 8453 or a Varian Cary 500 spectrophotometer. The concentrations of the peptides and copper(II) used to record absorption spectra were the same as those for the potentiometric titrations. Combined spectroscopic and potentiometric metal-complex titrations were performed into a 3 ml quartz cuvette with a 1 cm path length to get the spectrum in the visible region at each pH value simultaneously. These experiments were replicated at least three times for each copper(II)-peptide system. Spectroscopic data were processed by using the HYPERQUAD program [67].

2.4.2. CD measurements

CD spectra were obtained at 25 °C under a constant flow of nitrogen on a Jasco model 810 spectropolarimeter at a scan rate of 50 nm min^{-1} and a resolution of 0.1 nm. The path lengths were 1 or 0.1 cm, in the 190–800 nm range. The spectra were recorded as an average of 10 or 20 scans. Calibration of the instrument was performed with a 0.06% solution of ammonium camphorsulfonate in water. The CD spectra of

the copper(II) complexes on varying the solution pH were obtained in both the 240–400 and 300–800 nm wavelength regions. All the solutions were freshly prepared using double distilled water. The copper(II) ion and peptide concentrations used for the acquisition of the CD spectra in the visible region were identical to those used in the potentiometric titrations. CD spectra in the regions 240–400 were acquired by using copper(II) ion and peptide concentrations of 5.0×10^{-4} M. Far UV CD spectra were acquired by using Cu^{2+} ion and peptides concentrations ranging from 5.0×10^{-6} to 1.0×10^{-5} M and by using Zn^{2+} ion and peptides concentrations from 1.0×10^{-5} M to 1.0×10^{-4} M. The results are reported as ε (molar adsorption coefficient) and $\Delta\varepsilon$ (molar dichroic coefficient) in $M^{-1} cm^{-1}$.

2.4.3. EPR measurements

A Bruker Elexsys E500 CW-EPR (CW = continuous wave) spectrometer driven by a PC running XEpr program under Linux and equipped with a Super-X microwave bridge, operating at 9.3–9.5 GHz, and a SHQE cavity was used for all EPR experiments. All EPR spectra of frozen solutions of copper(II) complexes were recorded at 150 K by means of a ER4131VT variable temperature apparatus. EPR magnetic parameters were obtained directly from the experimental EPR spectra, always calculating them from the 2nd and the 3rd lines to get rid of second order effects. Instrumental settings of EPR spectra recordings of the copper(II)-peptide complexes were as follow: number of scans of 1–5; microwave frequency of 9.344–9.376 GHz; modulation frequency of 100 kHz; modulation amplitude of 0.2–0.6 mT; time constant of 164–327 ms; sweep time of 2.8 min; microwave power of 20–40 mW; receiver gain of $1 \times 10^4 - 2 \times 10^5$. Copper(II) complexes were prepared by addition of the appropriate amount of isotopically pure copper(II), taken from a $^{63}Cu(NO_3)_2$ 0.05 mol dm^{-3} solution, to the peptide solution. Copper(II) complex solutions were prepared in 10% methanol–water mixture to obtain a good quality glass upon freezing.

2.4.4. ESI-MS measurements

ESI-MS experiments were performed by using a Finnigan LCQ DECA XP PLUS ion trap spectrometer operating in the positive ion mode and equipped with an orthogonal ESI source (Thermo Electron Corporation, USA). Sample solutions were injected into the ion source at a flow-rate of 5 μl/min, using nitrogen as drying gas. The mass spectrometer operated with a capillary voltage of 46 V and capillary temperature of 250 °C, while the spray voltage was 4.3 kV.

2.5. Parallel tempering simulations

Ac-GHEITHG-NH_2 and Ac-GHTIEHG-NH_2 underwent 20 ns of parallel tempering (PT) simulations in explicit solvent with a total volume of $40 \times 40 \times 40$ Å^3, after having been equilibrated through 2 ns of MD in explicit solvent. GROMACS 4.5.5 package was used [69]. The overall charge of the system was neutralized by adding 1 sodium ion for the two systems. Periodic boundary conditions were applied. The AMBER99SB force field [70] was used for the biomolecules and counter ions, and the TIP3P force field [71] was used for water molecules. Electrostatic interactions were calculated using the Particle Mesh Ewald method [72]. A cutoff (0.9 nm) was used for the Lennard-Jones interactions. The time-step was set to 2 fs. All bond lengths were constrained to their equilibrium values using the SHAKE algorithm [73] for water and the LINCS algorithm [74] for the peptide. We simulated 64 replicas distributed in the temperature range of 300–500 K following a geometric progression. All replicas were simulated in NVT ensemble using a stochastic thermostat [75] with a coupling time of 0.1 ps. A thermostat that yields the correct energy fluctuations of the canonical ensemble is crucial in parallel tempering simulations [76]. Exchanges were attempted every 0.1 ps. The resulting average acceptance probability was 0.3 for all the replicas. The method of Daura and Van Gunsteren [77] was used in post-processing phase to cluster the resulting trajectories, with a cutoff of

1.5 Å calculated on the backbone atoms as implemented in the clustering utility provided in the GROMACS package [69].

The hydrogen bond percentage was calculated using a donor–acceptor distance cutoff of 3.5 Å and a cutoff of 60° in the angle formed by the donor–acceptor bond vectors [78]. All the structures are visualized using the VMD package [79].

2.6. Density functional theory calculations

The starting coordinates were considered from the four main PT clusters of Ac-GHEITHG-NH$_2$ and Ac-GHTIEHG-NH$_2$. To these coordinates copper(II) and zinc(II) ions were added. All density functional theory calculations (DFT) were performed using the Gaussian 09 program (revision C.01). The optimized geometries have been calculated using the PBE pseudopotential [80] for copper(II) and B3LYP pseudopotential for zinc(II) ion [81] and 6–31G* basis sets for each metal ions. For both complexes frequency calculations were performed to ensure that the geometries are local energy minima.

3. Results and discussion

3.1. Protonation constants and conformation features of Ac-GHEITHG-NH$_2$ and Ac-GHTIEHG-NH$_2$

Protonation constants of the two peptides were determined by potentiometric titrations (Table 1); the ligands show three proton accepting centers, as expected. The two protonation equilibria of the histidyl residues partly overlap and the average value for the protonation constants of the imidazole residues closely recalls that obtained for similar His-containing peptides [46]. Also the acidity of the glutamyl γ-carboxylic function nicely agrees with that found for other peptides containing glutamic residue [82,83]. The pK values of the carboxylate group are slightly different and appear to be affected by the position of the glutamic residues.

The far-UV CD spectra show that both peptides adopt predominantly a random coil conformation over the pH range investigated (4–10) (data not shown). The addition of Cu^{2+} induces significant changes in the conformation features of the two peptides; these variations are evident comparing the CD band profiles obtained by adding metal ion to the peptide solutions with those of the apo-subtracted difference spectra (Fig. 1).

The CD spectra differences (see inset Fig. 1A and B) indicate the formation of a metal-driven ordered conformation starting from pH 6 and 7 for Ac-GHEITHG-NH$_2$ and Ac-GHTIEHG-NH$_2$ peptides, respectively. In particular, the CD spectrum difference of Ac-GHEITHG-NH$_2$ peptide turns out to a typical turn CD spectrum, showing a clear Cotton splitting at 203 nm and two negative bands at 208 nm and 215 nm.

The Ac-GHTIEHG-NH$_2$ CD spectrum difference is also red-shifted with respect to the apo-peptide. Here, an asymmetric CD spectrum appears with one broad negative band centered at 206 nm and a shoulder centered at 218 nm.

Table 1
Protonation constants (logβ$_{pqr}$) and pK values for Ac-GHEITHG-NH$_2$ and Ac-GHTIEHG-NH$_2$ peptides (T = 298 K, I = 0.1 M KNO$_3$).[a]

Species	Ac-GHEITHG-NH$_2$	Ac-GHTIEHG-NH$_2$
	logβ$_{pqr}$	logβ$_{pqr}$
HL	6.77 (1)	6.78 (1)
H$_2$L	12.92 (1)	12.93 (1)
H$_3$L	16.99 (1)	17.06 (1)
pK His	6.77	6.78
pK His	6.15	6.15
pK COO$^-$	4.07	4.13

[a] Standard deviations (3σ values) are given in parentheses. Charges are omitted for clarity.
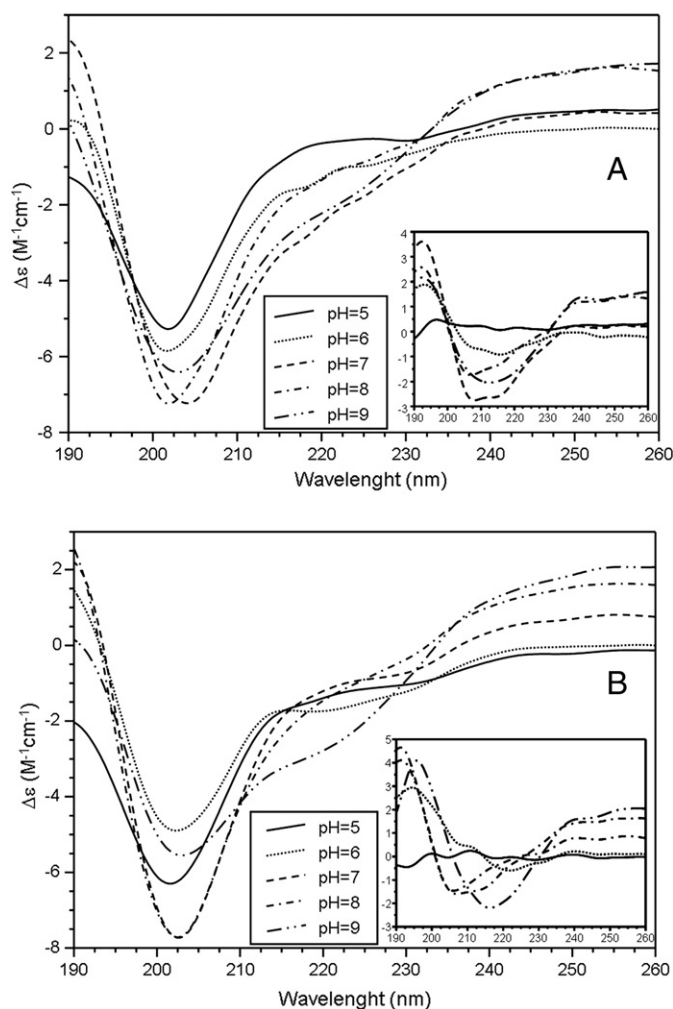

Fig. 1. Far-UV CD spectra at pH 5 (—), 6 (···), 7 (– – –), 8 (– · – ·) and 9 (– · · –) of copper(II) complexes with A) Ac-GHEITHG-NH$_2$ and B) Ac-GHTIEHG-NH$_2$ peptides. Inset: The apo subtracted difference spectra.

The experimental features of the CD spectra can be ascribed to the conformational selection [84] of metal ions which stabilize structured peptide domains.

The two minima disappear at pH 9 where a band characterized by a shallow minimum around 218 nm is evident, suggesting the formation of a prevailing turn conformation of the two peptides when the number of amide nitrogen deprotonation increases [85].

The addition of the zinc(II) does not determine a clear change in the secondary structure of both peptides (Fig. 2). This is probably due to the low percentage of complex species formation in the employed far-UV CD experiments.

The computational analysis of the two peptides secondary structures helped to rationalize the experimental data above reported.

The conformations of Ac-GHEITHG-NH$_2$ and Ac-GHTIEHG-NH$_2$ span unordered and turn domains, whose representative clusters are reported in Fig. 3. The turn sections are featured by i − i + 3 and i − i + 2 backbone hydrogen bonds, identifying the type I β-turn and γ-turn domains.

The former β-turn involves, for the Ac-GHEITHG-NH$_2$ peptide, the backbone oxygen of Glu3 and the backbone amide hydrogen of His6, while the γ-turn domain involves His2 and Ile4 residues.

The peptide Ac-GHTIEHG-NH$_2$ adopts different turn conformations. A γ-turn domain encompasses the acetyl carbonyl protecting Gly1 and the hydrogen amide of Thr3. The former γ-turn easily interconverts to a β-turn conformation between the acetyl carbonyl protecting Gly1 and the hydrogen amide of Ile4. A second β-turn domain is adopted between the carbonyl of His2 and the hydrogen amide of Glu5. A
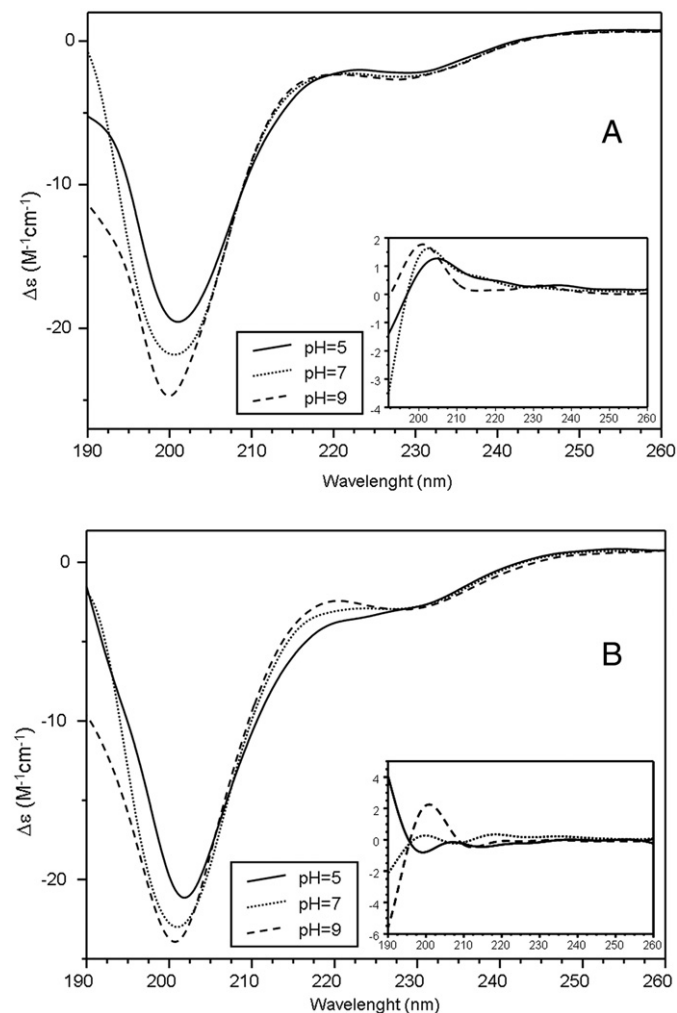
Fig. 2. Far-UV CD spectra at pH 5 (—), 7 (····) and 9 (– – –) of zinc(II) complexes with A) Ac-GHEITHG-NH₂ and B) Ac-GHTIEHG-NH₂ peptides. Inset: The apo subtracted difference spectra.

conformation with an $i - i + 5$ turn, typical of π-helixes, involving the acetyl carbonyl protecting Gly1 and the hydrogen amide of His6 is also adopted.

However, the backbone equilibria between unordered and turn domains are highlighted by the red-shift towards 203 nm observed in the CD spectra of both peptides.

Upon zinc(II) and copper(II) ions binding to peptides, the resulting CD spectrum differences highlight the adoption of structured peptide domains. The experimental features of the CD spectra, also in this case, can be ascribed to the conformational selection [84]; an effect due to the metal ions which induce stabilized structured peptide domains. In particular, the zinc(II) and copper(II) ions binding to the Ac-**GHEITHG**-NH₂ peptide determine the adoption of an extended conformation with a β-turn domain involving Ile4 and Gly7 (Fig. 4).

The presence of β-turn sections accounts for the intense Cotton splitting observed in the CD spectrum difference (see inset Fig. 1A).

The metal driven blue-shift of the Ac-**GHTIEHG**-NH₂ CD spectrum difference with respect to the Ac-**GHEITHG**-NH₂ peptide is due to the adoption of γ-turn domains [86] (Fig. 4), whose contribute is attributed to generally turn regions [87,88].

3.2. Speciation, stability constants, and coordination modes of Cu^{2+} and Zn^{2+} with Ac-GHEITHG-NH₂ and Ac-GHTIEHG-NH₂

The overall stability constants of the Cu^{2+} complexes are listed in Table 2, while the metal ion speciation for both peptides is shown in Fig. 5.

The first complex species formed by Ac-**GHEITHG**-NH₂ and Ac-**GHTIEHG**-NH₂ is $[CuHL]^{2+}$. The stepwise stability constant values calculated for these complex species ($\log K = \log\beta_{111} - \log\beta_{011}$) are 4.28 and 4.02 for Ac-**GHEITHG**-NH₂ and Ac-**GHTIEHG**-NH₂, respectively.

Both values are higher than those generally reported for the binding of only one imidazole nitrogen [37], suggesting that the γ-carboxylate functions of glutamyl residues also give a contribution to metal binding. The formation of macrochelate rings has been reported for similar systems where copper is coordinated to imidazole nitrogen and an aspartic carboxylate group [44,89,90]. The low formation percentages and the partly overlapping with the unprotonated complex formation (Fig. 5) do not allow for the determination of their spectral parameters.
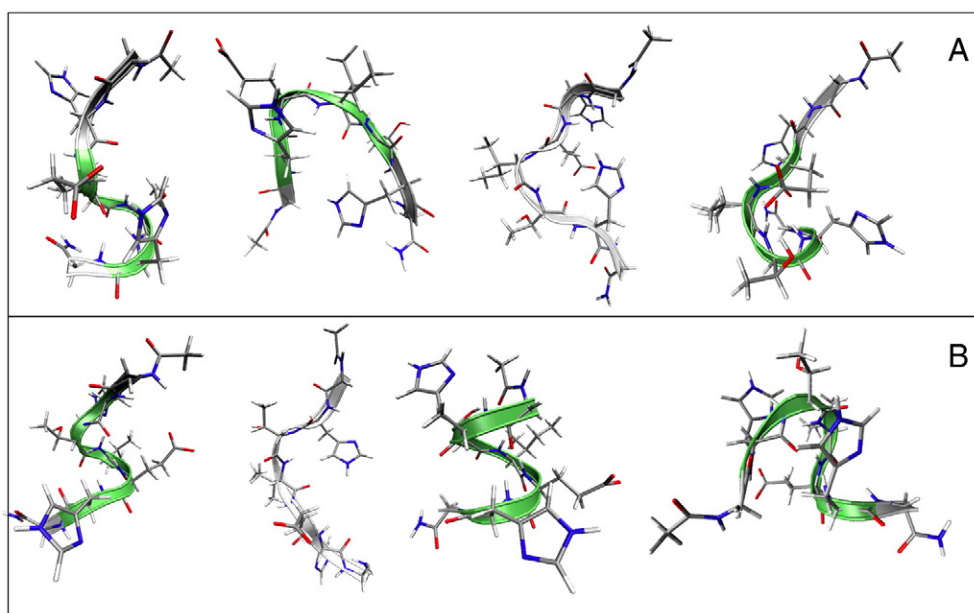

Fig. 3. The four main clusters of Ac-GHEITHG-NH₂ A) and Ac-GHTIEHG-NH₂ B). Turn domains are shown in green and unordered segments by silver ribbons. Carbon is shown in gray, nitrogen in blue and oxygen in red.

The predominant complex species at pH 6 is [CuL]$^+$. The stability constant value obtained for Ac-GHEITHG-NH$_2$ indicates the formation of a macrochelate with the involvement of the two imidazole nitrogen atoms and the glutamate carboxylate group, and it is similar to those reported for analogous peptides in which the metal ion displays the same 2N$_{im}$, COO$^-$, O$_{water}$ coordination environment [83,91].

The EPR parameters reported in Table 3 (g$_{||}$ = 2.298 and A$_{||}$ = 172×10^{-4}cm^{-1}), strongly support this hypothesis. The parallel hyperfine coupling constant value (A$_{||}$) is higher than those reported for other CuN$_2$O$_2$ chromophores, in which the metal is coordinated by two imidazole nitrogens and a carbonyl oxygen atom, being indicative of a stronger equatorial field due to the negative charge of the carboxylate oxygen [83,91,92].

UV–vis parameters obtained by spectroscopic titrations λ$_{max}$ = 655 nm (ε = 55) are consistent with the presence of a CuN$_2$O$_2$ chromophore with the metal ion bound to two nitrogen atoms and one carboxylate. CD spectra in the visible region show an extremely low intensity, confirming that the metal ion is coordinated with donor atoms belonging to the side chains which are more distant from chiral centers of peptide backbone. In particular, the CD spectrum at pH 6 of Cu-Ac-GHEITHG-NH$_2$ shows a wide d–d band centered at 624 nm with a relatively low intensity as found for other copper(II) complexes, in which the metal ion is bound to imidazole nitrogens and carboxylate group in a macrochelate ring [24,47].

The stability constant value of the analogous complex species [CuL]$^+$ formed by Ac-GHTIEHG-NH$_2$ is lower (logβ = 5.70) than that obtained

Table 2
Stability constants (logβ$_{pqr}$) and pK values of copper(II) complexes with Ac-GHEITHG-NH$_2$ and Ac-GHTIEHG-NH$_2$ peptides (T = 298 K, I = 0.1 M KNO$_3$).[a]

Species	Ac-GHEITHG-NH$_2$	Ac-GHTIEHG-NH$_2$
	logβ$_{pqr}$	logβ$_{pqr}$
CuHL	11.05 (4)	10.80 (4)
CuL	6.14 (2)	5.70 (2)
CuH$_{-1}$L	−0.70 (3)	−1.18 (4)
CuH$_{-2}$L	−7.98 (3)	−8.93 (3)
CuH$_{-3}$L	−17.47 (3)	−18.47 (5)
pK(1/0)	4.91	5.11
pK(0/−1)	6.84	6.88
pK(−1/−2)	7.28	7.75
pK(−2/−3)	9.49	9.54

[a] Standard deviations (3σ values) are given in parentheses. Charges are omitted for clarity; pK(n/m) values reflect the pK value of copper(II) complexes.

for the other peptide. This suggests the presence of a weakly bound carboxylate group to metal ion in addition to the two histidine imidazoles. The higher value of λ$_{max}$ = 680 and EPR parameters (see Table 3) confirms a weaker ligand field around copper(II) ion for the metal complex with Ac-GHTIEHG-NH$_2$, in comparison with the analogous species formed with Ac-GHEITHG-NH$_2$. Consistently, the CD signal at pH 6 is lower than that observed for Cu-Ac-GHEITHG-NH$_2$ system. These data confirm that the macrochelate formation is more favored in the sequence HEXXH in comparison with HXXEH one, even though the
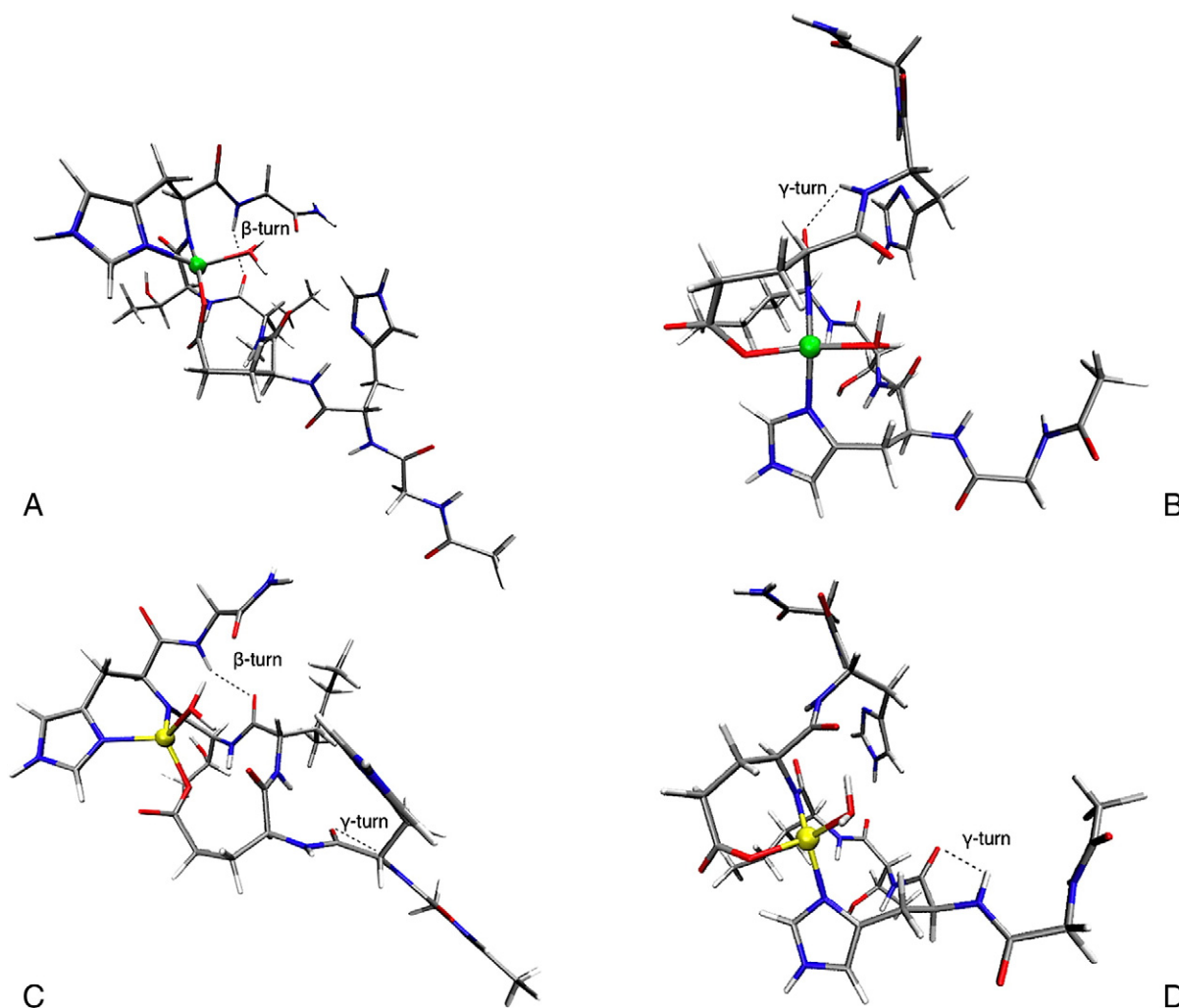

Fig. 4. The coordination of copper(II) and zinc ions within Ac-GHEITHG-NH$_2$ A), B) and Ac-GHTIEHG-NH$_2$ C). Copper(II) is shown in green, zinc ion in yellow, carbon in gray, nitrogen in blue and oxygen in red. β-Turn and γ-turn domains are highlighted by a silver line.
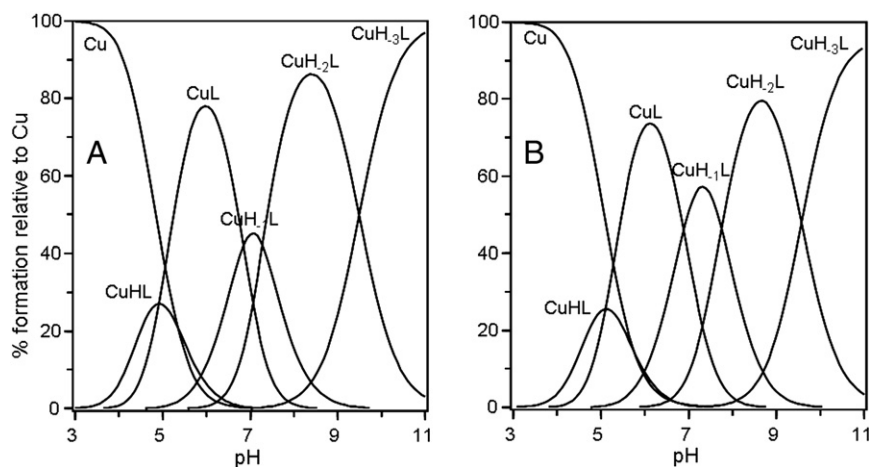
Fig. 5. Species distribution diagram for copper(II) complexes with Ac-GHEITHG-NH₂ and B) Ac-GHTIEHG-NH₂. Charges are omitted for clarity. [L] = 1 × 10⁻³ M; M/L molar ratio 1:1.

macrochelates in [CuL]⁺ species have the same dimension. This effect may also be influenced by the different conformational features of the two peptides and put into evidence that the relative position of glutamate residues within the sequence determines a lower stability constant for the [CuL] species formed with Ac-G**H**I**TE**H**G**-NH₂.

The [CuH₋₁L] formation overlaps with that of other species, thus its UV–vis and EPR parameters cannot be determined, though a blue shift in the UV–vis spectra is observed increasing the pH. Taking into account the pH range existence of this species, the deprotonation step involves an amide nitrogen atom. In comparison with the copper(II) complex with Ac-G**HE**I**TH**G-NH₂, the formation of the analogous copper(II) complex with Ac-G**H**T**IE**H**G**-NH₂ is shifted at higher pH and the maximum percentage of complex species reaches around the 60%. CD spectra carried out within pH 7–8 display both charge transfer band due to nitrogen amide deprotonation N⁻ → Cu²⁺ CT (319 nm) and to the imidazole CT, N_Im → Cu²⁺ CT band (352 nm), confirming the amide nitrogen deprotonation. This band is not evident in the copper(II) complex with Ac-G**HE**I**TH**G-NH₂ at pH 7 in agreement with the lower percentage formation of [CuH₋₁L] species.

The simultaneous presence of the [CuH₋₁L] and [CuH₋₂L]⁻ species hamper to identify unambiguously the metal coordination mode. Therefore, the investigation of the metal coordination properties by means of density functional theory (DFT) may result helpful to shed light on metal ion coordination environment. The coordination polyhedron parameters of the CuH₋₁L species are reported in Table 4 for both the Ac-G**HE**I**TH**G-NH₂ and Ac-G**H**T**IE**H**G-NH₂ peptides.

Analogously, the copper(II) coordination geometry in the same species formed with the Ac-**GH**T**IEH**G-NH₂ fragment is a type-II distorted tetragonal coordination geometry, involving the Nδ nitrogen of His2, the amide nitrogen of Glu5, the carboxyl group of Glu5 and a first shell coordination water (Table 4).

This coordination polyhedron accounts for a 7 membered ring within the carboxylate of Glu5 and its amide nitrogen. A macrochelate ring is also formed among the imidazole of His2 and the first shell coordination water weakly bound to the carbonyl group of His2.

The percentage of hydrogen bonds in the Ac-GHEITHG-NH₂ is higher than that calculated for the Ac-GHTIEHG-NH₂, and the intramolecular weak interactions increase upon copper(II) ion binding (Fig. 6). Noteworthy, this effect is larger for the [CuH₋₁L] species formed with Ac-GHTIEHG-NH₂ explaining the same pK values (6.84 and 6.88) obtained for the first deprotonation step (Table 2) even if the stability constant values of [CuL]⁺ species are different. Therefore copper(II) ion is able to select and stabilize fractions of structured protein sections.

[CuH₋₂L]⁻ is the main species above pH 8 (see Fig. 5). The pK values (7.28 and 7.75) indicate that the second deprotonation takes place, reasonably towards the N-termini so to form a [6 + 5 + 5] macrochelate and then involving the backbone of the second His residue in both peptides. However, the slight difference in stability constants between the two peptides further confirms the different levels of carboxylate binding in [CuL]⁺ species. The macrochelate formation with a (2N_Im,COO⁻, O_w) coordination mode delays the [CuH₋₁L] and [CuH₋₂L]⁻ formation, differently; the pK value of the second deprotonation step for the

Table 3
Spectroscopic parameters of copper(II) complexes with Ac-GHEITHG-NH₂ and Ac-GHTIEHG-NH₂ peptides. [L] = 1 × 10⁻³ M; molar ratio 1:1.

L	pH	Species	UV–vis* λ (nm) ε (M⁻¹ cm⁻¹))	CD λ (nm) (Δε (M⁻¹ cm⁻¹))	EPR g	A (10⁻⁴ cm⁻¹)
Ac-GHEITHG-NH₂	5	111,110	745 (22)	–		
	6	110	655 (55)	250 (0.377); 624 (−0.121)	2.298(1)	172(2)
	7	110,1−11		251 (1.322); 323 (0.115); 531 (0.066)	–	–
	8	1−11,1−21		253 (3.188); 294 (−0.08); 320 (0.310); 533 (0.133)		
	9	1−21	590 (90)	254 (3.550); 318 (0.531); 490 (−0.246); 627 (0.242);	2.227(1)	188(2)
	10	1−21, 1−31		258 (4.586); 316 (1.079); 356 (−0.290); 490 (−0.687); 633 (0.433)		
	11	1−31	525 (105)	259 (4.353); 315 (0.895); 358 (0.273); 498 (−0.705); 639 (0.336)	2.184(1)	193(2)
Ac-GHTIEHG-NH₂	5	111,110	744 (22)	–		
	6	110	680 (45)	257 (0.302)	2.308(4)	162(5)
	7	110,1−11,1−21		258 (0.716); 319 (0.070); 352 (−0,120); 530 (0.077)	–	–
	8	1−11, 1−21		259 (1.717); 320 (0.410); 362(−0.042); 550 (0.218)		
	9	1−21	580 (75)	259 (3.338); 319 (1.061); 489 (−0.411); 623 (0.301)	2.232(2)	188(3)
	10	1−21, 1−31		257 (5.504); 316 (1.489); 362 (−0.115); 491 (−0.785); 635 (0.505)		
	11	1−31	525 (108)	258 (6.365); 315 (1.671); 360 (−0.258); 496 (−0.795); 636 (0.512)	2.196(1)	191(2)

Errors in λ = ±2 nm and ε = 5%.

Table 4

Coordination parameters (Å and degree) for copper(II) polyhedra in Ac-GHEITHG-NH$_2$ and Ac-GHTIEHG-NH$_2$.

Parameter	Ac-GHEITHG-NH$_2$	Ac-GHTIEHG-NH$_2$
Distance (Å)		
Cu–N*$_{His6}$	1.96	–
Cu–N*$_{His2}$	–	2.01
Cu–N$_{amideHis6}$	1.92	–
Cu–N$_{amideGlu}$	–	1.92
Cu–O$_{Glu}$	1.93	1.88
Cu–O$_w$	2.03	2.04
N*$_{His6}$–Cu–N$_{amideHis6}$	88.2	–
N*$_{His2}$–Cu–N$_{amideGlu}$	–	152.9
N*$_{His6}$–Cu–O$_w$	134.28	–
N*$_{His2}$–Cu–O$_w$	–	98.1
O$_{Glu}$–Cu–O$_w$	92.5	142.9
N$_{amideHis6}$–Cu–O$_w$	97.5	–
N$_{amideGlu}$–Cu–O$_w$	–	95.1
N$_{His6}$–Cu–O$_{Glu}$	170.0	–
N$_{His2}$–Cu–O$_{Glu}$	–	86.8
Torsion (degree)		
Cu–N$_{amideHis6}$–C$_{\alpha His6}$–C$_{\beta His6}$	−23.5	–
Cu–N$_{amideGlu}$–C$_{\alpha Glu}$–C$_{\beta Glu}$	–	−27.0
Cu–N*$_{His6}$–C*$_{His6}$–C$_{\beta His6}$	−8.1	–
Cu–N*$_{His2}$–C*$_{His2}$–C$_{\beta His2}$	–	−9.5
O$_w$–Cu–N*$_{His6}$–C*$_{His6}$	55.8	–
O$_w$–Cu–N*$_{His2}$–C*$_{His2}$	–	4.3
Cu–O$_{Glu}$–C$_{Glu}$–C$_{\beta Glu}$	177.3	−39.5
O$_w$–Cu–N$_{amideHis6}$–C$_{Thr5}$	132.5	–
O$_w$–Cu–N$_{amideGlu}$–C$_{I5}$	–	113.9
Improper torsion (degree)		
N$_{amideHis6}$–O$_{Glu}$–N*$_{His6}$–O$_w$	−38.5	–
N$_{amideGlu}$–O$_{Glu}$–N*$_{His2}$–O$_w$		41.5

Fig. 6. Percentage of hydrogen bonds for Ac-GHEITHG-NH$_2$ and Ac-GHTIEHG-NH$_2$, upon coordinating Cu(II) and Zn(II) ions.

copper(II) complex with Ac-G**HEI**T**HG**-NH$_2$ is lower than that found for the analogous copper(II) complex with Ac-G**HTIEHG**-NH$_2$. The blue shifts which characterize the UV–vis spectroscopic parameters (see Table 3) are indicative of a CuN$_3$O$_1$ chromophore with the metal ion bound to one imidazole and two deprotonated amide nitrogens for both peptides. EPR and UV–vis suggest a possible weak interaction of carboxylate residue. In particular, the [CuH$_{−2}$L]$^−$ species formed by Ac-G**HTIEHG**-NH$_2$ display a superhyperfine structure on the first band of EPR spectra with a seven lines pattern in the pH range 7–9 (Fig. 7); this confirms the presence of three nitrogen donor atoms in the metal coordination equatorial plane. The CD band profile in the d–d transition region is different from that found in the physiologic pH range, with the positive band at λ$_{max}$ at 530 nm (Cu-Ac-G**HEI**T**HG**-NH$_2$ system) and at 550 nm (Cu-Ac-G**HTI**E**HG**-NH$_2$ system) that disappears while a negative band appears above pH 8 centered at 490 nm; this band intensity increases when the pH increases, characterizing the CD spectra of the successive copper(II) complexes. This behavior indicates a variation in the binding disposition of the second imidazole nitrogen outside from the equatorial plane.

This is different from that observed for other peptides containing two histidine residues [93], suggesting that the presence of glutamic acid between the two histidine residues may modify the coordination of the N-terminal histidine imidazole.

Increasing the pH, another species is formed, [CuH$_{−3}$L]$^{2−}$, which is the major complex species at pH values higher than 10. The blue-shift of UV–vis λ$_{max}$, the increase in the CD spectra of N$^−$ → Cu(II) charge transfer band at 315 nm and the EPR parameters clearly indicate the deprotonation of a third amide nitrogen.

The stability constant values of the complexes of Zn^{2+} with the two peptides are listed in Table 5.

The two peptides do not form any complex with Zn^{2+} up to pH 5 (see Fig. 8); above this pH the [ZnL]$^+$ species forms. The stability constant value for this complex species is similar in the two systems and it is indicative of the presence of two imidazole nitrogen atoms and a carboxylate group in the coordination sphere of Zn^{2+}. Such coordination
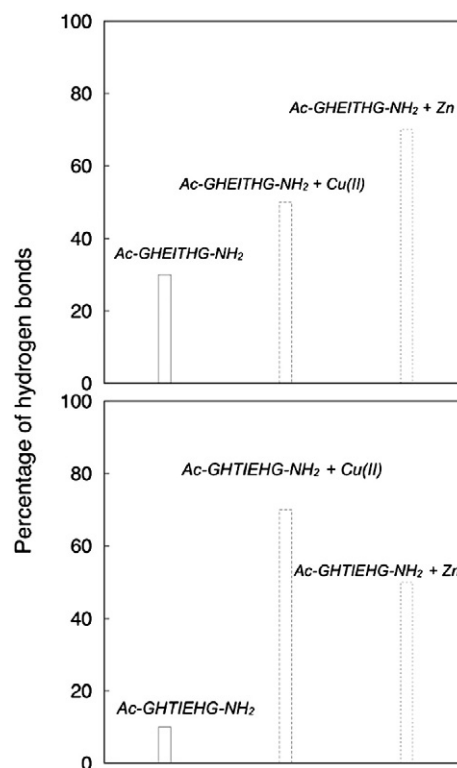
environment is also supported by the similarity between Zn-peptide binding constants values and that obtained for an analogous Zn^{2+} complexes of a N-terminus Aβ peptide fragment (log K$_{Aβ\ fragment}$ = 3.63); in the latter peptide the metal ion has been reported to be bound to two imidazole nitrogen atoms and to the carboxylate group of a Glu residue, leading to a macrochelate with a 2N1O (2N$_{Im}$,COO$^−$) binding mode [49]. At pH = 6, the [ZnH$_{−1}$L] complex species starts to form. In both cases the pK value suggests the deprotonation of an amide nitrogen atom. However, a large molar fraction (see Fig. 8) of uncomplexed metal ion is present over the entire pH range explored (3–6.5), it is responsible for the formation of a precipitate above pH 7 in the concentration ranges employed to perform reliable potentiometric measurements.

The ESI mass spectra of metal ions complex species have been carried out to put into light the eventual amide deprotonation [94]. The mass spectra characterization of the two peptides upon the addition of copper(II) confirm the formation of the 1:1 complex in both cases (data not shown). The [ZnL]$^+$ species (m/z = 853.40) is the main zinc(II) complex species at pH = 7.0 and it is detected in the ESI/MS spectrum acquired in positive ion mode (see Supplementary material). The solution pH could be increased up to 7.5 without any evidence of precipitation phenomena. This fact is due to the lower concentrations of ligand and metal ion than those used for potentiometric titrations. At pH 7.5, [ZnH$_{−2}$L]$^−$ (m/z = 851.35) is clearly detected as the main zinc(II) complex species in negative ion acquisition mode (Fig. 9). The matching between the experimental spectrum and the calculated isotopic distribution for [ZnH$_{−2}$L]$^−$ species definitely confirms that the main negatively charged metal complex species is not a hydroxo complex, but the metal ion with deprotonated amide nitrogen atoms in its coordination environment. This finding is observed for both peptides investigated.

Analogously to that observed for the [CuH$_{−1}$L], a computational approach was used to assign the binding details of [ZnH$_{−1}$L] complex species for their low percentage of formation. The coordination polyhedron parameters of the [ZnH$_{−1}$L] species are reported in Table 6 for both the Ac-G**HEI**T**HG**-NH$_2$ and Ac-G**HTI**E**HG**-NH$_2$ peptides.
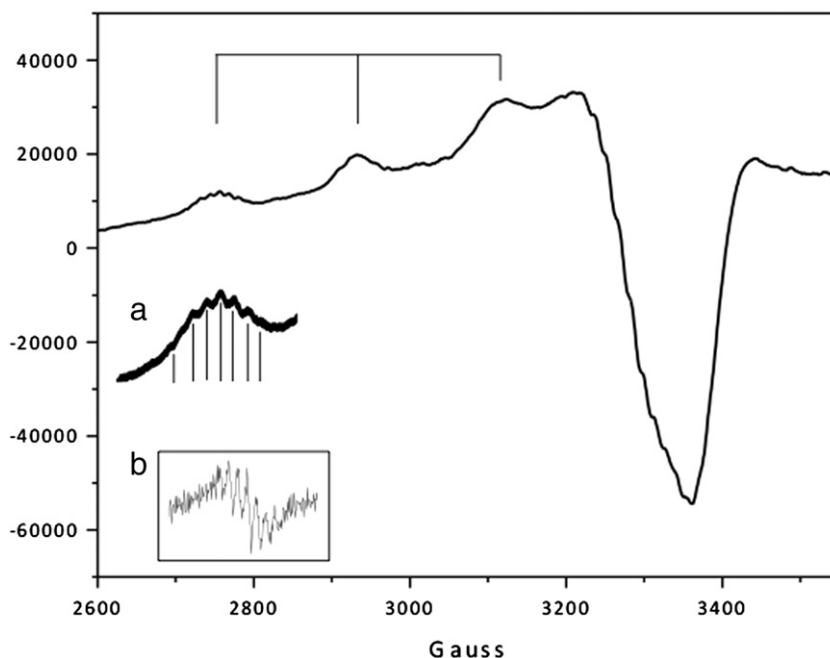
Fig. 7. Aqueous frozen solution EPR spectra at 150 K, pH 8, of the copper(II) complex with Ac-GHTIEHG-NH$_2$ ([L] = [Cu^{2+}] = 1.5 × 10^{-3} M). Microwave frequency = 9.344−9.376 GHz; modulation frequency = 100 kHz; modulation amplitude = 0.2–0.6 mT; sweep time = 2.8 min; microwave power = 20–40 mW. Inset: a) enlargement and b) first-derivative of the 1st band EPR spectrum.

Table 5
Stability constants (logβ$_{pqr}$) and pK values of zinc(II) complexes with Ac-GHEITHG-NH$_2$ and Ac-GHTIEHG-NH$_2$ peptides (T = 298 K, I = 0.1 M KNO$_3$).[a]

Species	Ac-GHEITHG-NH$_2$	Ac-GHTIEHG-NH$_2$
	logβ$_{pqr}$	logβ$_{pqr}$
ZnL	3.76 (2)	3.63 (2)
ZnH$_{-1}$L	−3.90 (7)	−4.20 (9)
ZnH$_{-2}$L	−11.38 (2)	−11.29 (2)
pK(0/−1)	7.65	7.82
pK(−1/−2)	7.48	7.09

[a] Standard deviations (3σ values) are given in parentheses. Charges are omitted for clarity; pK(n/m) values reflect the pK value of zinc(II) complexes.

The minimum energy structures of the former complexes predicted through DFT are reported in Fig. 4C and D. Intriguingly, zinc ion coordinates in a tetrahedral arrangement within Ac-GHEITHG-NH$_2$ and Ac-GHTIEHG-NH$_2$ peptides with the same donor atoms of copper(II). Those are the Nδ nitrogen of His6, the amide nitrogen of His6, the carboxyl group of Glu3 and a first shell coordination water for Ac-GHEITHG-NH$_2$ as well as the Nδ nitrogen of His2, the amide nitrogen of Glu5, the carboxyl group of Glu5 and a first shell coordination water for Ac-GHEITHG-NH$_2$ peptide. The coordination geometry of the former zinc complexes is quite close.

In particular, in line with copper(II), the intramolecular weak interactions increase upon zinc ion binding to Ac-GHEITHG-NH$_2$ and Ac-GHTIEHG-NH$_2$ peptides. Intriguingly, at variance with copper(II) which stabilizes in high amount the bent Ac-GHTIEHG-NH$_2$ peptide in comparison with the free ligand, zinc ion seems to stabilize more the elongated Ac-GHEITHG-NH$_2$ fragment (see Fig. 6).

4. Concluding remarks

Combined experimental and computational approaches have been employed to characterize the metal binding of HExxH and HxxEH
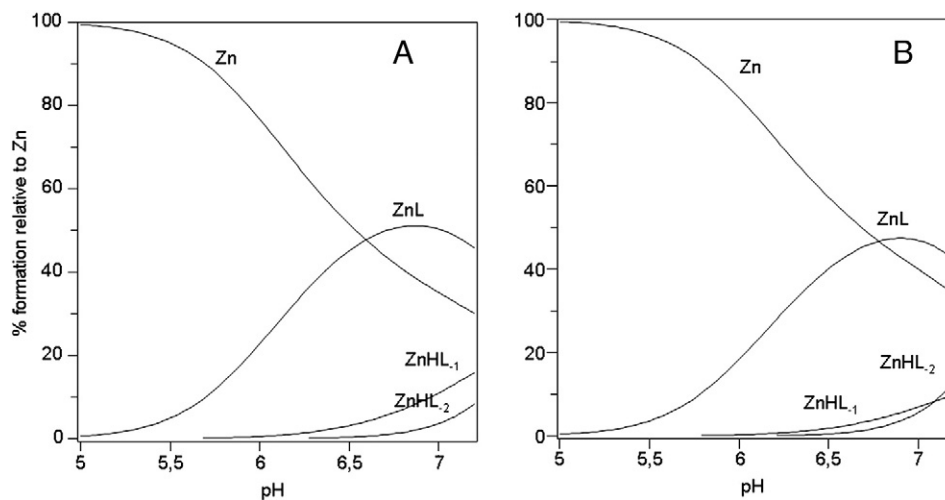

Fig. 8. Species distribution diagram for zinc(II) complexes with Ac-GHEITHG-NH$_2$ and B) Ac-GHTIEHG-NH$_2$. Charges are omitted for clarity. [L] = 1 × 10^{-3} M; M/L molar ratio 1:1.
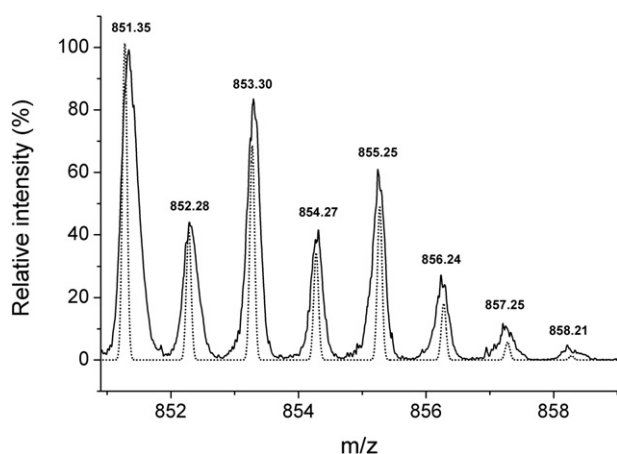
Fig. 9. ESI-MS spectrum obtained in the zoom scan and negative acquisition mode for the zinc(II)–Ac-GHTIEHG-NH$_2$ complex at pH 7.5. [L] = 1×10^{-5} M; M/L molar ratio 1:1. The experimental spectrum (solid line) is plotted along with the calculated isotopic distribution for the amide deprotonated [ZnH$_{-2}$L]$^-$ species (dotted line). The same spectrum was registered for the analogous complex species formed with the peptide Ac-GHEITHG-NH$_2$.

peptides, two motifs encompassing the catalytic site of zincin and inverzincin, respectively. Interestingly, copper(II) ions are known to inhibit IDE (inverzincin) whereas have no effect on neprilysin (NEP, zincin) [58]. ESI-MS results unambiguously indicate that the two peptides form amide deprotonated complex species also with zinc(II) ions, an uncommon behavior with multihistidine ligands [91].

In addition, computational approach evidences the metal-driven conformation of the two ligands in some complex species, which cannot be experimentally characterized for their low percentage of formation. Moreover, the presence of different hydrogen bonding networks between the copper(II) and zinc(II) complexes with the two peptides was determined. Results point to a significant contribution of such non-covalent interactions to the stability constant values, favorable in terms of additional bonds and unfavorable in terms of "stiffening" effect. Finally, the location of glutamate residue along the amino acid sequence of the investigated peptides appears to influence the thermodynamic and spectroscopic features of the complexes formed by the two ligands encompassing the HExxH and HxxEH binding motifs. The coordination of the two metals influences the hydrogen bond network. Both the contribution of additional non-covalent interactions and the dissimilar main species conformation drive the trend in the stability constant values. The different location of glutamate, reflected in the metal affinity, suggests the need of a further deep investigation about the role of Asp/Glu residues along multi-histidine sequences.

Acknowledgment

Table 6
Coordination parameters (Å and degree) for zinc polyhedra in Ac-GHEITHG-NH$_2$ and Ac-GHTIEHG-NH$_2$.

Parameter	Ac-GHEITHG-NH$_2$	Ac-GHTIEHG-NH$_2$
Distance (Å)		
Zn–N*$_{His6}$	2.03	–
Zn–N*$_{His2}$	–	2.04
Zn–N$_{amideHis6}$	1.99	–
Zn–N$_{amideGlu}$	–	1.95
Zn–O$_{Glu}$	1.97	1.93
Zn–O$_w$	2.03	2.05
N*$_{His6}$–Zn–N$_{amideHis6}$	94.6	–
N*$_{His2}$–Zn–N$_{amideGlu}$	–	135.2
N*$_{His6}$–Zn–O$_w$	117.7	–
N*$_{His2}$–Zn–O$_w$	–	106.3
O$_{Glu}$–Zn–O$_w$	103.0	103.7
N$_{amideHis6}$–Zn–O$_w$	106.7	–
N$_{amideGlu}$–Zn–O$_w$	–	106.0
N$_{His6}$–Zn–O$_{Glu}$	111.3	–
N$_{His2}$–Zn–O$_{Glu}$	–	91.6
Torsion (degree)		
Zn–N$_{amideHis6}$–C$_{\alpha His6}$–C$_{\beta His6}$	−13.9	–
Zn–N$_{amideGlu}$–C$_{\alpha Glu}$–C$_{\beta Glu}$	–	−35.9
Zn–N*$_{His6}$–C*$_{\gamma His6}$	−20.5	–
Zn–N*$_{His2}$–C*$_{\gamma His2}$	–	−16.8
O$_w$–Zn–N*$_{His6}$–C*$_{His6}$	85.0	–
O$_w$–Zn–N*$_{His2}$–C*$_{His2}$	–	−11.0
Zn–O$_{Glu}$–C$_{Glu}$–C$_{\beta Glu}$	−71.9	−80.0
O$_w$–Zn–N$_{amideHis6}$–C$_{Thr5}$	124.8	–
O$_w$–Zn–N$_{amideGlu}$–C$_{I5}$	–	119.6
Improper torsion (degree)		
N$_{amideHis6}$–O$_{Glu}$–N*$_{His6}$–O$_w$	−67.43	–
N$_{amideGlu}$–O$_{Glu}$–N*$_{His2}$–O$_w$		64.3

References

[1] G. Henkel, B. Krebs, Chem. Rev. 104 (2004) 801–824.
[2] B. Ruttkay-Nedecky, L. Nejdl, J. Gumulec, O. Zitka, M. Masarik, T. Eckschlager, M. Stiborova, V. Adam, R. Kizek, Int. J. Mol. Sci. 14 (2013) 6044–6066.
[3] H. Xiao, K.T. Jeang, J. Biol. Chem. 273 (1998) 22873–22876.
[4] M.D. Michelitsch, J.S. Weissman, Proc. Natl. Acad. Sci. U. S. A. 97 (2000) 11910–11915.
[5] A. Mangeon, R.M. Junqueira, G. Sachetto-Martins, Plant Signal. Behav. 5 (2010) 99–104.
[6] P. Thandopani, T.R. O'Connor, T.L. Bailey, S. Richard, Mol. Cell 50 (2013) 613–623.
[7] N. Barker, S. Tan, H. Clevers, Development 140 (2013) 2484–2494.
[8] Y. Jaillais, Y. Belkhadir, E. Balsemao-Pires, J.L. Dangl, J. Chory, Proc. Natl. Acad. Sci. U. S. A. 108 (2011) 8503–8507.
[9] S. Pujals, E. Giralt, Adv. Drug Deliv. Rev. 60 (2008) 473–484.
[10] M. Scocchi, A. Tossi, R. Gennaro, Cell. Mol. Life Sci. 68 (2011) 2317–2330.
[11] X. Ren, J.H. Hurley, Traffic 12 (2011) 1282–1290.
[12] S. Cun, Y. Lai, Y. Chang, H. Sun, Metallomics 5 (2013) 904–912.
[13] Y.D. Sharma, Int. J. Biochem. 20 (1988) 471–477.
[14] Y.D. Sharma, Comp. Biochem. Physiol. B 98 (1991) 433–435.
[15] J.L. Zehnder, L.L. Leung, J. Lab. Clin. Med. 125 (1995) 682–683.
[16] A.L. Jones, M.D. Hulett, C.R. Parish, Immunol. Cell Biol. 83 (2005) 106–118.
[17] H. Wake, S. Mori, K. Liu, H.K. Takahashi, M. Nishibori, Eur. J. Pharmacol. 623 (2009) 89–95.
[18] K. Poon, K.K. Poon, K.K. Patel, D.S. Davis, C.R. Parish, M.D. Hulett, Blood 117 (2011) 2093–2101.
[19] S.Y. Huang, Y.C. Chen, Anal. Chem. 85 (2013) 3347–3354.
[20] R. Ge, Y. Zhang, X. Sun, R.M. Watt, Q.Y. He, J.D. Huang, D.E. Wilcox, H. Sun, J. Am. Chem. Soc. 128 (2006) 11330–11331.
[21] S. Cun, H. Li, R. Ge, M.C.M. Lin, H. Sun, J. Biol. Chem. 283 (2008) 15142–15151.
[22] Y. Zeng, N. Yang, H. Sun, Chem. Eur. J. 17 (2011) 5852–5860.
[23] J.A. Hayden, M.B. Brophy, L.S. Cunden, E.M. Nolan, J. Am. Chem. Soc. 135 (2013) 775–787.
[24] D. La Mendola, A. Magrì, A.M. Santoro, V.G. Nicoletti, E. Rizzarelli, J. Inorg. Biochem. 111 (2012) 59–69.
[25] A. Myari, G. Malandrinos, Y. Deligiannakis, J.C. Plakatouras, N. Hadjiliadis, Z. Nagy, I. Sovago, J. Inorg. Biochem. 85 (2001) 253–261.
[26] J. Brasun, C. Gabbiani, M. Ginanneschi, L. Messori, M. Orfei, J. Swiatek-Kozlowska, J. Inorg. Biochem. 98 (2004) 2016–2021.
[27] G. Arena, R.P. Bonomo, G. Impellizzeri, R.M. Izatt, J.D. Lamb, E. Rizzarelli, Inorg. Chem. 26 (1987) 795–800.
[28] C. Kallay, K. Varnagy, G. Malandrinos, N. Hadjiliadis, D. Sanna, I. Sovago, Dalton Trans. (2006) 4545–4552.
[29] J. Brasun, M. Cebrat, A. Sochacka, O. Gładysz, J. Swiatek-Kozłowska, Dalton Trans. (2008) 4978–4980.
[30] M. Pietruszka, E. Jankowska, T. Kowalik-Jankowska, Z. Szewczuk, M. Smuzynska, Inorg. Chem. 50 (2011) 7489–7499.
[31] H. Czapor, S. Bielińska, W. Kamysz, Ł. Szyrwiel, J. Brasuń, J. Inorg. Biochem. 105 (2011) 297–302.
[32] A. Kolozsi, A. Jancso, N.V. Nagy, T.J. Gajda, Inorg. Biochem. 103 (2009) 940–947.
[33] A. Fragoso, P. Lamosa, R. Delgado, O. Iranzo, Chem. Eur. J. 19 (2013) 2076–2088.
[34] M. Kuczer, M. Błaszak, E. Czarniewska, G. Rosinski, T. Kowalik-Jankowska, Inorg. Chem. 52 (2013) 5951–5961.
[35] S. Rajkovic, C. Kallay, R. Serenyi, G. Malandrinos, N. Hadjiliadis, D. Sanna, I. Sovago, Dalton Trans. (2008) 5059–5071.
[36] A. Kolozsi, I. Vosekalna, T. Martinek, E. Larsen, B. Gyurcsik, Dalton Trans. (2009) 5647–5654.
[37] H. Kozłowski, W. Bal, M. Dyba, T. Kowalik-Jankowska, Coord. Chem. Rev. 183 (1999) 319–346.
[38] I. Sovago, K. Osz, Dalton Trans. (2006) 3841–3854.
[39] I. Sovago, C. Kallay, K. Varnagy, Coord. Chem. Rev. 256 (2012) 2225–2233.

[40] V. Joszai, I. Turi, C. Kallay, G. Pappalardo, G. Di Natale, E. Rizzarelli, I. Sovago, J. Inorg. Biochem. 112 (2012) 17–24.
[41] D. Valensin, L. Szyrwiel, F. Camponeschi, M. Rowinska-Zyrek, E. Molteni, E. Jankowska, A. Szymanska, E. Gaggelli, G. Valensin, H. Kozlowski, Inorg. Chem. 48 (2009) 7330–7340.
[42] D. La Mendola, R.P. Bonomo, S. Caminati, G. Di Natale, S.S. Emmi, Ö. Hansson, G. Maccarrone, G. Pappalardo, A. Pietropaolo, E. Rizzarelli, J. Inorg. Biochem. 103 (2009) 195–204.
[43] E. Gaggelli, H. Kozlowski, D. Valensin, G. Valensin, Chem. Rev. 106 (2006) 1995–2044.
[44] T. Karavelas, G. Malandrinos, N. Hadjiliadis, P. Mlynarz, H. Kozlowski, M. Barsam, I. Butler, Dalton Trans. (2008) 1215–1223.
[45] C. Kallay, K. Osz, A. David, Z. Valastyan, G. Malandrinos, N. Hadjiliadis, I. Sovago, Dalton Trans. (2007) 4040–4047.
[46] S. Timári, C. Kállay, K. Osz, I. Sóvágó, K. Várnagy, Dalton Trans. (2009) 1962–1971.
[47] C. Kallay, K. Varnagy, G. Malandrinos, N. Hadjiliadis, D. Sanna, I. Sovago, Inorg. Chim. Acta 362 (2009) 935–945.
[48] Z. Paksi, A. Jancsó, F. Pacello, N. Nagy, A. Battistoni, T. Gajda, J. Inorg. Biochem. 102 (2008) 1700–1710.
[49] C.A. Damante, K. Osz, Z. Nagy, G. Pappalardo, G. Grasso, G. Impellizzeri, E. Rizzarelli, I. Sovago, Inorg. Chem. 48 (2009) 10405–10415.
[50] B. Amrein, M. Schmid, G. Collet, P. Cuniasse, F. Gilardoni, F.P. Seebeck, T.R. Ward, Metallomics 4 (2012) 379–388.
[51] K. Fukasawa, K.M. Fukasawa, H. Iwamoto, J. Hirose, Biochemistry 38 (1999) 8299–8303.
[52] G. Grasso, M.L. Giuffrida, E. Rizzarelli, Metallomics 4 (2012) 937–949.
[53] C. Ciaccio, G.F. Tundo, G. Grasso, G. Spoto, D. Marasco, M. Ruvo, S. Marini, E. Rizzarelli, M. Coletta, J. Mol. Biol. 385 (2009) 1556–1567.
[54] F. Bellia, A. Pietropaolo, G. Grasso, J. Mass Spectrom. 48 (2013) 135–140.
[55] G. Grasso, E. Rizzarelli, G. Spoto, J. Mass Spectrom. 44 (2009) 735–741.
[56] G. Grasso, E. Rizzarelli, G. Spoto, BBA Proteins Proteomics 1784 (2008) 1122–1126.
[57] G. Grasso, F. Salomone, G.R. Tundo, G. Pappalardo, C. Ciaccio, G. Spoto, A. Pietropaolo, M. Coletta, E. Rizzarelli, J. Inorg. Biochem. 117 (2012) 351–358.
[58] G. Grasso, A. Pietropaolo, G. Spoto, G. Pappalardo, G.R. Tundo, C. Ciaccio, M. Coletta, E. Rizzarelli, Chem. Eur. J. 17 (2011) 2752–2762.
[59] K.M. Fukasawa, T. Hata, Y. Ono, J. Hirose, J. Amino Acids 1 (2011)(Article ID: 574816).
[60] I. Bertini, G. Canti, H. Kozlowski, A. Scozzafava, J. Chem. Soc. Dalton Trans. 8 (1979) 1270–1273.
[61] R.C. Rosenberg, C.A. Root, P.K. Bernstein, H.B. Gray, J. Am. Chem. Soc. 97 (1975) 2092–2096.
[62] P.S.T. Tan, K.M. Pos, W.N. Konings, Appl. Environ. Microbiol. 57 (1991) 3593–3599.
[63] J. Hirose, T. Ohsaki, N. Nishimoto, S. Matuoka, T. Hiromoto, T. Yoshida, T. Minoura, H. Iwamoto, K.M. Fukasawa, Biol. Pharm. Bull. 29 (2006) 2378–2382.
[64] J. Hirose, H. Iwamoto, I. Nagao, K. Enmyo, H. Sugao, N. Kanemitu, K. Ikeda, M. Takeda, M. Inoue, T. Ikeda, F. Matsuura, K.M. Fukasawa, K. Fukasawa, Biochemistry 40 (2001) 11860–11865.
[65] D. La Mendola, R.P. Bonomo, G. Impellizzeri, G. Maccarrone, G. Pappalardo, E. Rizzarelli, A. Pietropaolo, V. Zito, J. Biol. Inorg. Chem. 10 (2005) 463–475.
[66] G. Arena, R. Calì, E. Rizzarelli, S. Sammartano, R. Barbucci, M.J.M. Campbell, J. Chem. Soc. Dalton Trans. (1978) 1090–1094.
[67] P. Gans, A. Sabatini, A. Vacca, Talanta 43 (1996) 1739–1753.
[68] L. Alderighi, P. Gans, A. Ienco, D. Peters, A. Sabatini, A. Vacca, Coord. Chem. Rev. 184 (1999) 311–318.
[69] B. Hess, J. Chem. Theory Comput. 4 (2008) 116–122.
[70] V. Hornak, R. Abel, A. Okur, B. Strockbine, A. Roitberg, C. Simmerling, Proteins 65 (2006) 712–725.
[71] W.L. Jorgensen, J. Chandrasekhar, J.D. Madura, R.W. Impey, M.L. Klein, J. Chem. Phys. 79 (1983) 926–935.
[72] U. Essmann, L. Perera, M.L. Berkowitz, T. Darden, H. Lee, L.G. Pedersen, J. Chem. Phys. 103 (1995) 8577–8593.
[73] S. Miyamoto, P.A. Kollman, J. Comput. Chem. 13 (1992) 952–962.
[74] B. Hess, C. Kutzner, D. van der Spoel, D. Lindahl, J. Chem. Theory Comput. 4 (2008) 435–447.
[75] G. Bussi, D. Donadio, M. Parrinello, J. Chem. Phys. 126 (2007) 014101.
[76] E. Rosta, N.V. Buchete, G. Hummer, J. Chem. Theory Comput. 5 (2009) 1393–1399.
[77] X. Daura, K. Gademann, B. Jaun, D. Seebach, W.F. van Gunsteren, A.E. Mark, Angew. Chem. Int. Ed. 38 (1999) 236–240.
[78] W. Kabsch, C. Sander, Biopolymers 22 (1983) 2577–2637.
[79] W. Humphrey, A. Dalke, K. Schulten, J. Mol. Graphics 14 (1996) 33–38.
[80] J. Perdew, K. Burke, M. Ernzerhof, Phys. Rev. Lett. 77 (1996) 3865–3868.
[81] A.D. Becke, J. Chem. Phys. 98 (1993) 5648–5652.
[82] C. Kállay, K. Várnagy, G. Micera, D. Sanna, I. Sóvágó, J. Inorg. Biochem. 9 (2005) 1514–1525.
[83] A. Travaglia, G. Arena, R. Fattorusso, C. Isernia, D. La Mendola, G. Malgieri, V.G. Nicoletti, E. Rizzarelli, Chem. Eur. J. 17 (2011) 3726–3738.
[84] D.D. Boehr, R. Nussinov, P.E. Wright, Nat. Chem. Biol. 5 (2009) 789–796.
[85] G. Di Natale, G. Grasso, G. Impellizzeri, D. La Mendola, G. Micera, N. Mihala, Z. Nagy, K. Osz, G. Pappalardo, V. Rigo, E. Rizzarelli, D. Sanna, I. Sovago, Inorg. Chem. 44 (2005) 7214–7225.
[86] A. Motta, M. Reches, L. Pappalardo, G. Andreotti, E. Gazit, Biochemistry 44 (2005) 14170–14178.
[87] A. Perczel, G.D. Fasman, Proteins Sci. 1 (1992) 378–395.
[88] E. Vass, Z. Majer, K. Kohalmy, M. Hollósi, Chirality 22 (2010) 762–771.
[89] B. Boka, A. Myari, I. Sovago, N. Hadjiliadis, J. Inorg. Biochem. 98 (2004) 113–122.
[90] D. La Mendola, A. Magrì, Ö. Hansson, R.P. Bonomo, E. Rizzarelli, J. Inorg. Biochem. 103 (2009) 758–765.
[91] C. Kallay, Z. Nagy, K. Varnagy, G. Malandrinos, N. Hadjiliadis, I. Sovago, Bioinorg. Chem. Appl. (2007) 9, (ID 30394).
[92] D. La Mendola, A. Magrì, T. Campagna, M.A. Campitiello, L. Raiola, C. Isernia, Ö. Hansson, R.P. Bonomo, E. Rizzarelli, Chem. Eur. J. 16 (2010) 6212–6223.
[93] D. La Mendola, D. Farkas, F. Bellia, A. Magrì, A. Travaglia, Ö. Hansson, E. Rizzarelli, Inorg. Chem. 51 (2012) 128–141.
[94] P. Mineo, D. Vitalini, D. La Mendola, E. Rizzarelli, E. Scamporrino, G. Vecchio, J. Inorg. Biochem. 98 (2004) 254–265.